Available online at www.sciencedirect.com
SCIENCE DIRECT®
Acta Biomaterialia 1 (2005) 387–397
Acta BIOMATERIALIA
www.actamat-journals.com

Self-assembling peptide amphiphile nanofiber matrices for cell entrapment

Elia Beniash [1], Jeffery D. Hartgerink [2], Hannah Storrie, John C. Stendahl, Samuel I. Stupp *

Department of Materials Science and Engineering, Chemistry and the Feinberg School of Medicine, Northwestern University, Evanston, IL 60208, USA

Received 28 December 2004; received in revised form 29 March 2005; accepted 6 April 2005

Abstract

We have developed a class of peptide amphiphile (PA) molecules that self-assemble into three-dimensional nanofiber networks under physiological conditions in the presence of polyvalent metal ions. The assembly can be triggered by adding PA solutions to cell culture media or other synthetic physiological fluids containing polyvalent metal ions. When the fluids contain suspended cells, PA self-assembly entraps cells in the nanofibrillar matrix, and the cells survive in culture for at least three weeks. We also show that entrapment does not arrest cell proliferation and motility. Biochemical and ultrastructural analysis by electron microscopy indicate that entrapped cells internalize the nanofibers and possibly utilize PA molecules in their metabolic pathways. These results demonstrate that PA nanofibrillar matrices have the potential to be used for cell transplantation or other tissue engineering applications.

1. Introduction

The rapidly developing field of regenerative medicine [1–5] will require rational molecular and supramolecular design of temporary scaffold materials for cells to control their bioactivity and physical properties. In our view, along with biocompatibility requirements, these synthetic materials also need to resemble biological extracellular matrices and interact with cells at molecular level in order to effectively control the processes of tissue regeneration. Developments in the field of materials chemistry [1–9] now offer synthetic strategies for biomimetic materials to meet the challenges of designing artificial extracellular matrices. The use of self-assembly to generate hierarchical supramolecular structures [10–12] is a biomimetic strategy now receiving growing attention in the field of biomaterials [13–16]. One group of novel materials for tissue engineering applications are peptide-based self-assembling fibrous networks [6,7,9,16,17]. Our laboratory has developed a series of peptide amphiphile (PA) molecules as materials for tissue engineering [6–9]. These amphiphilic molecules are composed of a peptide segment containing 6–12 amino acids coupled via an amide bond to a fatty acid chain that varies in length from 10 to 22 carbon atoms. At concentrations as low as 0.25% by weight [6,7], these molecules self-assemble into self-supporting gels. The gels are formed by a network of cylindrical nanofibers, ranging from 5 to 8 nm in diameter, depending on the length of the self-assembling molecules that form them. The basic building block of these networks, a nanofiber, forms with the hydrophobic alkyl tails of the molecules at its core and the hydrophilic peptide segments comprising the outer surface [6,7]. Our laboratory has previously reported on peptide amphiphile nanofiber

* Corresponding author. Tel.: +1 847 491 3002; fax: +1 847 491 3010.
E-mail address: s-stupp@northwestern.edu (S.I. Stupp).
[1] EB is currently at the Department of Biomineralization, The Forsyth Institute, Boston, MA.
[2] JDH is currently at the Department of Chemistry, Rice University, Houston, TX.

1742-7061/$ - see front matter © 2005 Acta Materialia Inc. Published by Elsevier Ltd. All rights reserved.
doi:10.1016/j.actbio.2005.04.002

networks that can be mineralized with hydroxyapatite to recreate the nanoscale structure of bone [6], and we have recently reported on the use of bioactive peptide amphiphile nanofibers to promote rapid and selective differentiation of neural progenitor cells into neurons [9].

In our original work on these systems, self-assembly was induced through pH change [6]; however, PA supramolecular assemblies produced by this method are unstable at physiological pH unless they are internally cross-linked through covalent bonds. Recently, we reported on a new approach to self-assemble PA molecules into nanofibers at physiological pH based on the electrostatic attraction of molecules containing opposite charge [8]. Formation of intermolecular bonds through metal ions has been shown to be a powerful strategy for supramolecular assembly and aggregation in natural and synthetic systems [18–20]. In this paper, we describe the mechanism of metal ion mediated self-assembly of PA molecules at physiological pH and its applications in cell entrapment.

2. Materials and methods

2.1. Synthesis of peptide amphiphiles (PAs)

PAs were synthesized using a method previously described [6,7]. Briefly, automated, Fmoc-protected solid-phase peptide synthesis was used to produce the peptide portion of the molecule followed by a manual coupling reaction to couple the N-terminus of the peptide to palmitic acid via the formation of an amide bond. The structure of a PA molecule is shown in Fig. 1 and a list of the PA molecules used in this study is shown in Table 1.

2.2. Formation of PA gels

A basic assessment of self-assembly was conducted for PA molecules **1**–**8**. Self-assembly was induced by the addition of 1 M solutions of NaCl, KCl, $MgCl_2$, $CaCl_2$, $BaCl_2$, $ZnBr_2$, $Cu(ClO_4)_2$, and $GdCl_3$ to 200 μL volumes of 10 mM aqueous PA solutions at pH 7.5 (Table 1). The final metal ion concentrations were 20 mM for polyvalent ions and 200 mM for monovalent ions. In addition, 10 mM solutions of PA molecules **1** and **2** were exposed to KCl and NaCl at concentrations up to 6 M. The effect of polyvalent metal salt concentration on PA **1** and **2** assembly was also assessed with 5–50 mM $GdCl_3$ and $CaCl_2$. Finally, in order to test the ability of physiological solutions to induce assembly, 10 mM PA solutions were mixed with equal amounts of the following: minimum essential medium alpha (MEMα) with 10% fetal bovine serum (FBS), Dulbecco's modified Eagle's medium (DMEM) with 10% FBS, phosphate buffered saline (PBS) without Ca^{2+} and Mg^{2+}, and Hank's balanced salt solution (HBSS) without Ca^{2+} and Mg^{2+} (Gibco). Mechanical integrity of the self-assembled materials was gauged by their ability to resist gravitational stresses when the vials were inverted. "Self-supporting gels" were identified as those that remained attached to the bottom of the vial for at least 30 s with little or no observable viscous flow. Materials with primarily viscous character were defined as

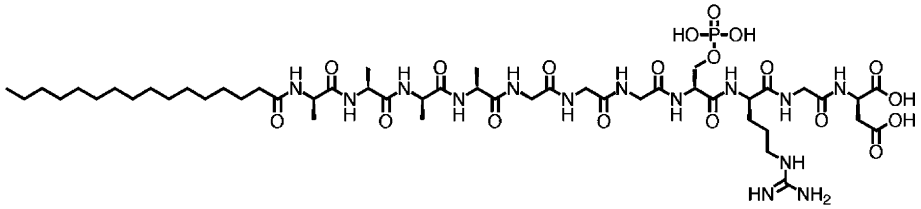

Fig. 1. Chemical structure of RGD-containing PA molecule **1**.

Table 1
Gelation of peptide amphiphiles with metal cations; 10 mM aqueous PA solutions were mixed with cations and the gelation behavior was observed

PA	Sequence	Charge	K^{+a}	Mg^{2+b}	Ca^{2+}	Ba^{2+}	Cu^{2+}	Zn^{2+}	Gd^{3+}
1	Alkyl-$C_4G_3S^{(P)}$RGD-COOH	−3	Viscous liquid	Gel	Gel	Gel	N/A	Gel	Gel
2	Alkyl-$A_4G_3S^{(P)}$RGD-COOH	−3	Viscous liquid	Gel	Gel	Gel	Gel	Gel	Gel
3	Alkyl-$A_4G_3S^{(P)}$KGE-COOH	−3	Viscous liquid	Gel	Gel	Gel	Gel	Gel	Gel
4	Alkyl-C_4G_3SRGD-COOH	−1	Viscous liquid	Viscous liquid	Gel	Gel	N/A	Gel	Gel
5	Alkyl-A_3G_2EQS-COOH	−2	Viscous liquid	Gel	Gel	Gel	Gel	Gel	Gel
6	Alkyl-A_4G_3ERGDS-COOH	−2	Viscous liquid	Viscous liquid	Viscous liquid	Viscous liquid	N/A	Gel	Gel
7	Alkyl-C_4G_3EIKVAV-COOH	−1	Gel	Gel	Gel	N/A	N/A	Gel	Gel
8	Alkyl-C_4G_3KIKVAV-NH_2	+2	Gel	Viscous liquid	Viscous liquid	Viscous liquid	N/A	Viscous liquid	Viscous liquid

[a] 200 mM KCl.
[b] 20 mM for all polyvalent cations.

those that exhibited observable viscous flow upon inversion.

2.3. Oscillating rheometry

Materials formed by self-assembly of PA molecule **3** were examined via oscillatory rheology. Data were collected with a Paar Physica Modular Compact Rheometer 300 operating in a 20 mm parallel plate configuration. All samples contained 120 μL of 2 wt.% solution of **3** added to the bottom plate. Assembly was initiated by gradually pipetting 60 μL of 60 mM aqueous ion solutions while stirring with the pipette tip (final ion concentrations 20 mM). The following ion salts were tested: KCl, $MgCl_2$, $CaCl_2$, $BaCl_2$, $CuCl_2$, $ZnBr_2$, and $GdCl_3$. After mixing, the top plate was lowered onto samples to a gap distance of 0.5 mm. The stage temperature was maintained at 25 °C and a hydrated chamber containing saturated tissues was placed around gels to minimize evaporation. All samples were allowed to equilibrate 30 min before testing at 3% oscillatory strain from 100 to 0.1 rad/s. Storage moduli (G'), loss moduli (G''), and complex viscosities (η^*) were averaged over a minimum of two trials and plotted versus angular frequency with errors of one standard deviation.

2.4. FTIR studies

For FTIR studies, PA gels were lyophilized and mounted in KBr pellets. Spectra were collected on a Bio-Rad FTS-40 FTIR spectrometer at a resolution of $2\ cm^{-1}$, with 32 scans for each sample. Spectra were analyzed using the program Microcal Origin 6.0.

2.5. Cell culture

MC3T3-E1 cells were maintained in MEMα media supplemented with 10% fetal bovine serum and 1% penicillin/streptomycin in T25 culture flasks at 37 °C and 5% CO_2. For encapsulation experiments, 10 mg/mL PA solutions in distilled water were filtered through 0.25 μm syringe filters, sterilized under UV light overnight, and then 100 μL of PA solution was placed in each chamber of an eight well multi-chamber slide (Fisher). Cells were trypsinised, centrifuged, re-suspended at a density of 20,000 cells/mL, and supplemented with $CaCl_2$ to bring the Ca^{2+} concentration in the medium to 10 mM. Cell suspension (100 μL) was added to each well of the multi-chamber slide and mixed with the PA solution. Immediately upon mixing, the viscosity of the solution increased, effectively entrapping the cells in the PA matrix. The slides were then placed into a 37 °C incubator for 30 min for maturation of the nanofibrillar matrix, after which time, 0.5 mL of cell media was added to each well of the multi-chamber slide. Media exchanges were made every fourth day. In control experiments, the cells were grown in the wells of the multichamber slides in the absence of PA nanofibrillar matrices.

2.6. TEM studies

Acellular nanofibrillar assemblies for TEM studies were prepared by standard techniques described previously [6,7]. For matrices containing cells, the gels were prefixed, with 2% glutaraldehyde in MEMα medium without FBS or antibiotics, directly in the multichamber slides for 1 h at 4 °C. Samples were then fixed in modified Karnovsky fixative (2% glutaraldehyde, 2% formaldehyde, 0.1 M cacodylate buffer, pH 7.5) for 5 h at room temperature, followed by 12 h at 4 °C. After fixation, samples were washed with 0.1 M cacodylate buffer twice for 30 min, post-fixed with 1% OsO_4 in 0.1 M cacodylate buffer for 30 min at room temperature and then rinsed in 0.1 M cacodylate buffer for 10 min and twice with distilled water for 10 min. Samples were then removed from the multichamber slide, placed into 20 mL glass vials and dehydrated twice for 20 min in a sequence of 20%, 40%, 70%, and 95% ethanol solutions and twice for 10 min in 100% ethanol. For embedding, samples were incubated twice for 10 min in propylene oxide, transferred to a 1:1 mixture of propylene oxide and Spipon 812 embedding resin (SPI), and left in closed vials for 12 h followed by 8 h in open vials. Samples were then transferred into pure Spipon, and left at ambient temperature for 24 h, with one resin exchange, after which time, samples were transferred into fresh resin and polymerized at 40, 50 and 70 °C for 24 h each. Finally, samples were cut using a diamond knife (Diatome) on the Leica Ultracut ultramicrotome. The sections were contrasted with 1% lead citrate and 2% uranyl acetate and examined on a JEOL 100C electron microscope at 100 kV.

2.7. Light microscopy

Samples were monitored during the experiments using a Nikon TE200 inverted microscope equipped with a Spot RT CCD camera controlled with Metamorph digital analysis software at magnifications 200× and 400×. For viability assays, cell were reacted with LIVE/DEAD reagent (Molecular Probes) for 15 min at 37 °C, rinsed and imaged using an epifluorescence attachment on a Nikon TE200 inverted microscope.

2.8. Cell proliferation assay

Cell proliferation assays were carried out based on the method of Allen et al. [21]. Briefly, two PA gels containing cells were removed from cultures at selected time points stored at −80 °C until all samples could be assayed together. Cells were digested in papain

(0.125 mg/mL, Sigma) with 0.1 M cysteine in PBE buffer (pH 6.5) at 60 °C for 16 h. The digested samples (5 μL) were reacted with 195 μL Hoechst 33258 dye in TNE buffer (0.1 μg/mL, pH 7.5, Molecular Probes) and fluorescence emission at 460 nm (with excitation at 346 nm) was monitored on a Molecular Devices Gemini EM fluorescence plate reader. All data were collected using Costar opaque white clear bottom 96-well plates (Fisher), and each measurement repeated in triplicate. Total DNA in each sample was determined from a calibration curve of intensity vs. DNA content of calf thymus DNA, and the number of cells was calculated by estimating 7.7 ng of DNA per cell [22].

2.9. Analysis of cellular metabolism

Glucose and lactate concentration were measured in the media from PA experiments as well as in initial media and media from the controls using a YSI 2700 Select Biochemical Analyzer. The media from three experimental multichamber slides and two controls were analyzed every four days upon media exchange. For each multichamber slide, the media from all eight wells was mixed together and then analyzed. The media was collected with sterile syringes, filtered through 0.2 μm syringe filters (Whatman) and analyzed immediately after collection.

3. Results and discussion

3.1. Studies of metal ion triggered PA assembly at physiological conditions

Metal ions are a common component of body fluids and cell culture media and are used in a number of cell entrapment systems to trigger gelation [23,24]. We have previously briefly described the ability of the PA molecules to assemble into nanofibers in the presence of calcium ions [7]. In the present work, we have studied this mode of self-assembly in depth, using a broad range of the PA molecules, as well as a number of metal ions, with special focus on the basic mechanisms of this assembly and structural organization of the nanofibrils. We have examined the potential of several PA molecules to assemble in the presence of metal ions. PA molecule **3** was studied in detail with oscillatory rheology to gain a better perspective of the material's mechanical properties when self-assembly is triggered by different metal ions. Rheological data indicate that all PA **3** specimens prepared with polyvalent metal ions formed gels. In each mechanical spectrum, G′ and G″ were only minimally sensitive to ω, with G′ constantly greater than G″ (Fig. 2). This confirms that these materials are gels with predominately elastic character, rather than viscous liquids. On the other hand, G″ was consistently greater than G′ in specimens prepared with monovalent ions,

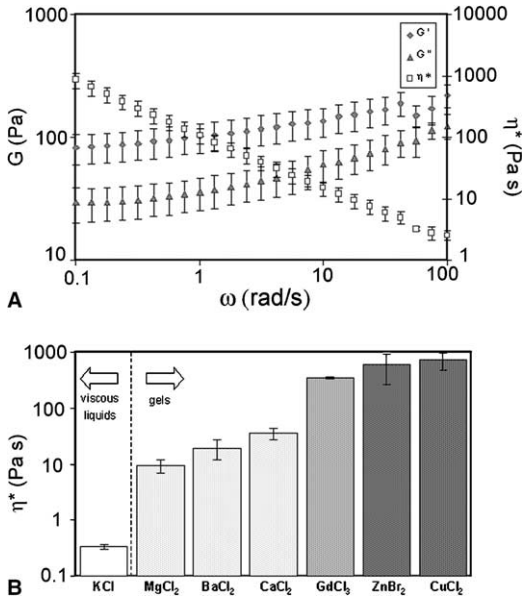

Fig. 2. (A) Mechanical spectrum for gels of PA molecule **3** prepared with 20 mM $MgCl_2$. (B) Complex viscosities at $\omega = 17.8$ rads^{-1} for PA molecule **3** assembled with various ion salts.

and thus, these materials are more appropriately classified as viscous liquids. Among gels of PA **3** prepared with different polyvalent ions, there were significant differences in moduli (Fig. 2). Gels prepared with alkaline earth metals had significantly lower moduli than those prepared with transition metals. Overall, however, the mechanical properties of PA gels formed with polyvalent metal ions appear to be comparable to those of biopolymer gels [25,26] and self-assembled peptide gels [27].

Results of inverted vial experiments to gauge self-assembly in PA molecules **1**–**8** are summarized in Table 1. In general, self-assembly behavior of other negatively charged PAs was similar to that which was observed for **3**. With the exception of PA molecule **7**, negatively charged PAs did not form self-supporting gels in the presence of KCl at a molar ratio of 1:20. Further experiments showed that 10 mM solutions of molecules **1** and **2** did not form self-supporting materials even in the presence of 6 M KCl or NaCl. However, most negatively charged PAs were found to form self-supporting gels in the presence of polyvalent metal ions, such as Ca^{2+}, Mg^{2+}, and Cu^{2+}. Thus, it appears that polyvalent ions are significantly more effective initiators of self-assembly than monovalent species. For the dilutions of molecules **1** and **2** used in these experiments, the minimum concentrations of polyvalent ions required for assembly of self-supporting gels appears to be roughly equal to the molarity of PA molecules. In contrast to PAs **1**–**6**, IKVAV-containing molecules **7** and **8** were shown to form self-supporting gels at KCl concentrations of 200 mM. Interestingly, molecule **8**, which is positively charged and does not contain any acidic amino acids, did not form self-supporting gels upon addition

of polyvalent metal ions. This suggests that interactions between acidic groups in PAs **1**–**6** and positively charged counterions play a key role in their self-assembly. The ability of molecules **7** and **8** to form self-supporting gels in the presence of monovalent ions may be related to the sequence of their peptides. The IKVAV sequence features the hydrophobic amino acids isoleucine and valine interspersed among the more hydrophilic residues alanine and lysine. Since the side chains of adjacent amino acids are located on opposite sides of the peptide backbone, this sequence should facilitate intermolecular contact of like components. This effect may enhance the driving force for self-assembly via close association of hydrophobic side chains. Amphiphilic peptides have been previously shown to assemble into ribbon-like structures, forming 3-D networks upon addition of monovalent salts [28,29].

The gels formed by addition of polyvalent metal ions to PA solutions are remarkably stable under a variety of conditions. In our experiments, $CaCl_2$ induced gels of molecules **1** and **2** were stable in a broad pH range from 4 to 11. In contrast, gels formed by the pH-triggered mechanism we reported earlier [6], are stable only below pH 3.5. Furthermore, metal ion triggered gels survive heating up to 100 °C, and only shrink slightly as temperature rises. This remarkable stability of the PA gels is in contrast with other hydrogels forming via ionic bonds with polyvalent metal ions such as, for example, Ca-alginate, which is stable only in the narrow pH window around neutrality and is affected by heating [30,31]. We surmise that such high stability of PA gels is determined by diversity of intermolecular interactions in the nanofibers, including hydrophobic, ionic and hydrogen bonds (see below). We have also found that gels of molecules **1** and **2** formed at a 2:1 ratio of metal ions to PA remain intact for at least 14 days when exposed to a volume of deionized water 10 times greater than the volume of the gel. These results suggest that strong interactions occur between polyvalent metal ions and PA molecules in the self-assembled state. Evidence for the formation of bonds between PA and metal ions is provided by gelation experiments in the presence of Cu^{2+} ions. We observed that addition of 20 mM $Cu(ClO_4)_2$ to 10 mM solutions of PA molecules **3** or **5** resulted in a color change from transparent to blue upon gelation. UV–Vis spectra of the gels show a 60-nm blue shift and an increase in intensity compared to aqueous solutions of $Cu(ClO_4)_2$ of the same concentration, suggesting formation of copper–peptide complexes [32,33].

Many of the metal cations tested as gelators for PA molecules are present in culture media used to maintain cells in vitro and in a variety of bodily fluids. By using cation-mediated PA gelation, we can trigger PA self-assembly upon contact with living tissues or upon addition of cell suspensions in culture medium in vitro. Self-supporting gels form upon mixing of equal volumes of cell culture media and aqueous solutions of molecules **2** and **3**. When solutions of molecules **2** and **3** were mixed with PBS or HBSS depleted of Ca^{2+} and Mg^{2+}, gelation was not observed. These experiments indicate that polyvalent metal ions present in cell culture media can induce self-assembly of negatively charged PAs.

3.2. Structural characterization of PA nanofibrillar assemblies

We have used transmission electron microscopy (TEM) to characterize the ultrastructural organization of metal-ion-induced PA gels. Electron micrographs of positively stained samples and resin embedded sections show that gels are comprised of three-dimensional networks of fibers that are 5–6 nm in diameter (Fig. 3). This is consistent with our previous measurements of dehydrated nanofibers [6]. Analysis of TEM micrographs of positively stained nanofibers assembled directly on a TEM grid reveal that uranyl acetate stains only peripheral parts of nanofibers, while the core remains unstained (Fig. 3A). TEM of resin embedded sections of a gel assembled in culture medium shows the same organization (Fig. 3B and C). Additionally, micrographs of fibers sectioned transversely have a doughnut appearance, with an unstained central part and an intensely stained outer circle (Fig. 3D). Since uranyl acetate stains mainly charged groups and does not react with saturated hydrocarbons, these TEM data demonstrate further that in the presence of polyvalent metal ions, PA molecules assemble into nanofibers with their aliphatic tails in the core and peptide segments on the periphery. This structural organization of the metal ion-induced PA nanofibers is similar to that of nanofibers formed by pH changes [6].

FTIR spectroscopy of the metal ion-induced PA gels was carried out in order to characterize the conformation of peptide segments in the nanofibers. The observation of an amide A band located near 3290 cm^{-1} indicates formation of strong hydrogen bonding in the nanofibers, and the position of the amide I band maximum between 1630 and 1640 cm^{-1} in all samples (Fig. 4A), indicates that the peptide segments in the nanofibers adopt a mainly β-sheet conformation [34,35]. At the same time, no secondary peaks were observed around 1690 cm^{-1}, which suggests a parallel β-sheet arrangement [34,36]. Given that the peptide chains comprising β-sheets are parallel to each other [34,37], we assume that the planar peptide groups should be co-aligned with the long axes of the nanofibers (Fig. 4B and C). Most importantly, in contrast to well-known cylindrical micelles formed by common surfactants [38–41], these nanofibers display their hydrophilic segments with a significant degree of order, determined by the inter-chain hydrogen bonds and ionic interactions [42–44].

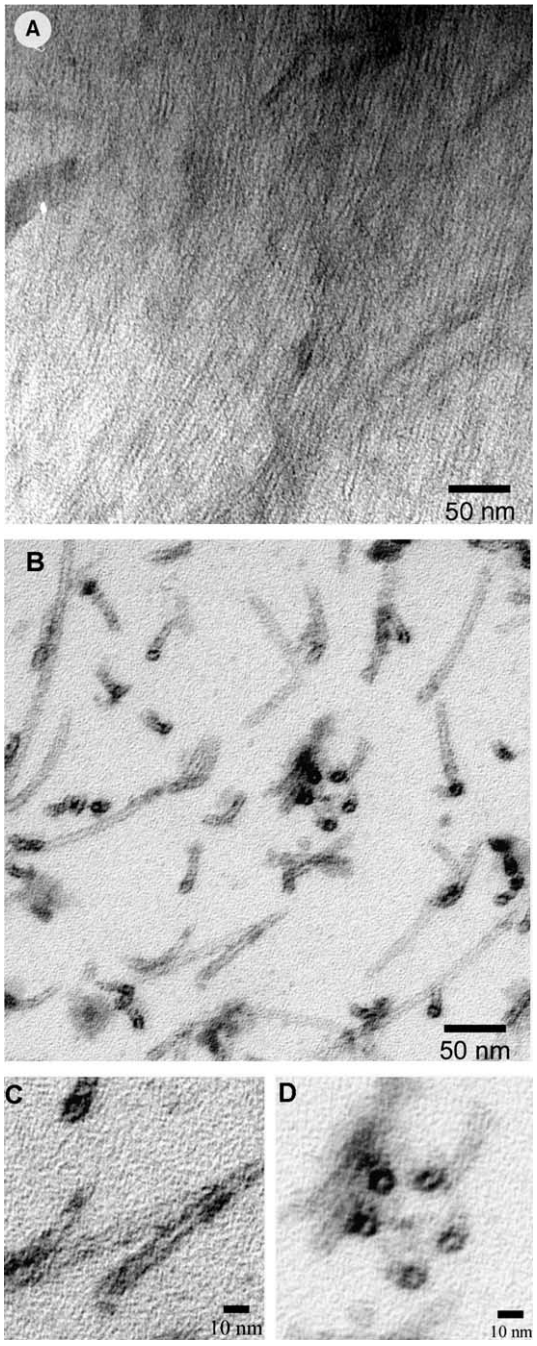

Fig. 3. TEM micrographs of metal-induced PA gels. (A) Gel formed by addition of 20 mM of $CaCl_2$ to a 10 mM solution of molecule **2** directly on a TEM grid. (B) Section of PA nanofiber matrix formed by mixing solution of molecule **3** with culture medium embedded in resin and stained with uranyl acetate. (C) Close up showing two nanofibers in the plane of the section, with electron dense peripheries and transparent cores. (D) Close up of PA matrix revealing nanofiber cross sections, with intensively stained peripheries and unstained core.

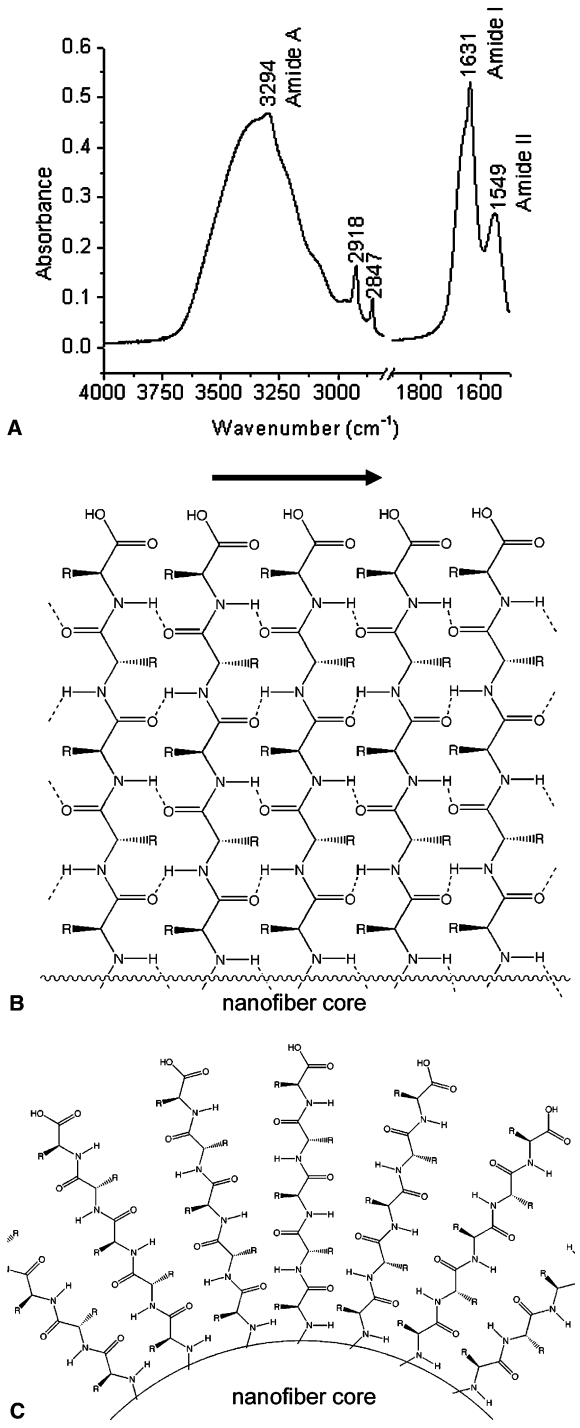

Fig. 4. (A) FT-IR spectrum of a gel formed by addition of 20 mM $CaCl_2$ to a 10 mM solution of molecule **2**. (B) Schematic representation of the parallel arrangement of peptide chains in the plane parallel to the long axis of a nanofiber essential for formation of β-sheet. (C) Schematic representation of the cross section of a nanofiber showing that the peptide chains cannot form highly hydrogen bonded network.

3.3. Cell entrapment in PA nanofibrillar matrix

We have previously studied neuron progenitor cells entrapped in the gel formed by molecule **7**, which contains laminin signaling motif [9]. As mentioned above the mechanism of assembly of molecules **7** and **8** is different from other PA molecules, and requires amphiphilic peptide motifs. In the present study, we focused on cell entrapment in PA gels assembled via interactions

with polyvalent metal ions. We primarily focused here on general properties of the PA nanofibrillar matrices as materials for cell entrapment and not on the effect of specific signaling motifs on cell behavior.

PA molecules **3** and **5** were chosen for cell entrapment experiments because they do not contain any known cell adhesion or signaling sequences. The C-terminal sequence of molecule **3** is Lys-Gly-Glu (KGE), which has a charge distribution similar to the integrin binding motif Arg-Gly-Asp (RGD) [45]. It has been reported that substitution of the Asp residue for Glu in RGD reduces the cell-binding activity of the peptide by more than 100-fold [46]; therefore, we assume that KGE sequences on nanofibers will have no specific integrin binding activity. The sequence Glu-Gln-Ser (EQS) at the C-terminus of the molecule **5** was randomly selected, and as far as we know is not a cell adhesion or signaling epitope.

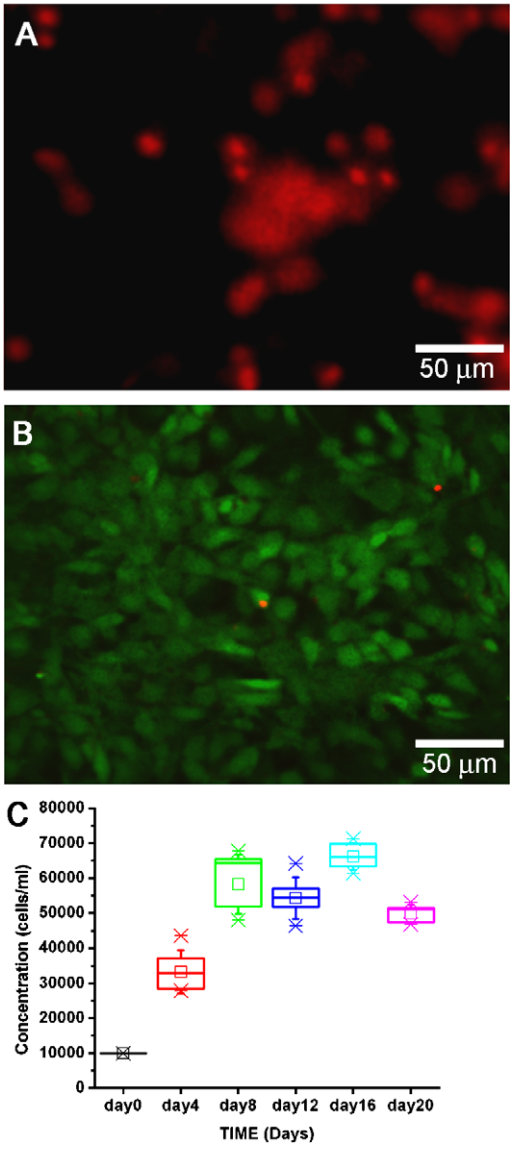

Fig. 5. Cell viability and proliferation in PA gels. (A) Fluorescent micrograph displaying a live-dead assay of MC3T3-E1 cells entrapped in a nanofibrillar matrix formed by molecule **5** after 20 days in culture. (B) Fluorescent micrograph displaying a live–dead assay of MC3T3-E1 cells entrapped in a nanofibrillar matrix formed by molecule **3** after 20 days in culture. (C) Box chart showing changes in concentration of cells embedded in a nanofibrillar matrix formed by molecule **3** during the course of the experiment. The box is the 75% distribution range; the error bars indicate one standard deviation.

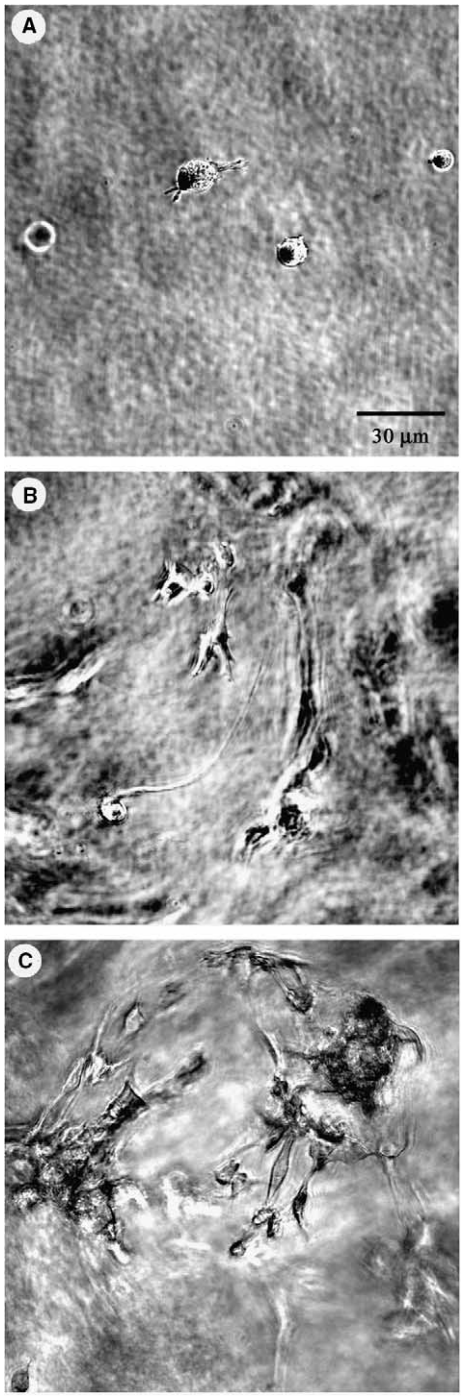

Fig. 6. Optical micrographs of MC3T3-E1 cells in a nanofibrillar matrix composed of molecule **3** after (A) 3 h; (B) 6 days and (C) 13 days in culture. All images were collected at the same magnification.

Cell behavior in nanofibers networks was dependent on the PA molecule used to form the network. Cells entrapped in EQS-terminated fibrils remained spherical for the duration of the experiment. The cells did not proliferate and the viability assay performed at day 20 of the experiment showed that all the cells were dead (Fig. 5A). In contrast, cells encapsulated in networks of KGE-terminated nanofibers survived and proliferated over the course of the experiment. A viability assay performed on cells after 20 days inside a KGE gel indicated that a vast majority of cells tolerate entrapment conditions reasonably well (Fig. 5B). Furthermore, cell density increases 6-fold during the first eight days reaching a plateau at ca. 60,000 cells/mL (Fig. 5C). These data indicate that cell entrapment in a KGE-containing PA nanofibrillar matrix does not arrest cell proliferation.

The morphology of cells encapsulated in KGE PA gels was observed by light microscopy. Cell morphology begins to change almost immediately after entrapment (Fig. 6A). Over time, a majority of cells lose their spherical appearance, adopt a spindle-like shape, aggregate and send processes to adjacent cells (Fig. 6B). The aggregation among cells becomes even more apparent throughout the duration of the experiment (Fig. 6C). Therefore, it is clear that the entrapment in the KGE nanofiber matrix does not arrest cell motility and aggregation.

TEM analysis of cells entrapped in a KGE matrix reveals a normal morphology (Fig. 7). The nuclei appear normal, while mitochondria and smooth and rough endoplasmic reticulum are abundant in the cells, implying high levels of metabolism and protein synthesis. Interestingly, TEM analysis reveals that cells readily internalize the nanofibers via endocytosis and accumulate them in membrane-delineated compartments, most likely lysosomes (Fig. 7B). The fact that cells internalize PA nanofibers has a number of important implications. First, it suggests that PA nanofibers can be degraded by

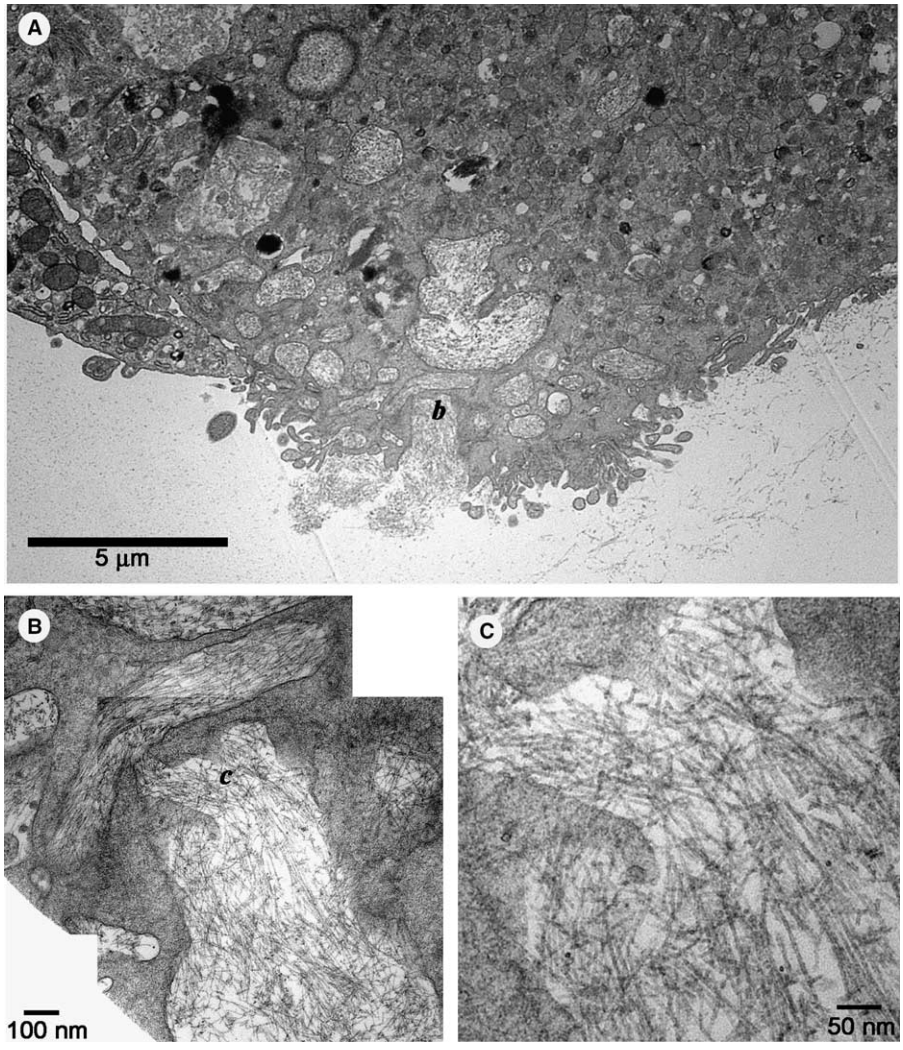

Fig. 7. (A) TEM micrograph of a cell entrapped in the nanofibrillar matrix internalizing the PA nanofibers. (B) Intermediate magnification of the region marked ***b*** in Fig. 5A showing the formation of intracellular membrane delineated compartments filled with nanofibers; (C) High magnification micrograph of the nanofibers in the area marked ***c*** in Fig. 5B.

natural mechanisms without being cytotoxic, which is crucial for in vivo tissue engineering applications. Secondly, it suggests that cells may be able to utilize the nanofibers in their metabolic pathways as a source of nutrients. The delivery of nutrients in developing artificial tissue is one of the challenges facing tissue regeneration. The limited availability of nutrients tends to limit the thickness of the artificial tissues that can be grown in vitro to a few cell layers [47,48].

In order to test the hypothesis that cells are able to metabolize PA molecules, we measured glucose and lactate concentrations in the culture medium after exposure to the cells entrapped by PA gels. The differences in glucose (ΔG) and lactate (ΔL) mass concentrations in culture media were used as a measure of metabolic activity of cultured cells [49–51]. In cell cultures, glycolysis is the major catabolic pathway [52,53], and in this pathway, two lactate molecules are formed per molecule of glucose consumed. Analysis of changes in concentrations of glucose and lactate in the media is widely used in basic studies of cell physiology [54,55], as well as in the fields of biotechnology [49,56–58] and tissue engineering [59–62] to monitor a metabolic activity in cell cultures. Since the molecular weight of lactic acid is half that of glucose, the mass of lactic acid produced in glycolysis is equal to the mass of glucose reacted. Therefore, under typical cell culture conditions the sum of ΔG and ΔL ($\Sigma_{\Delta G,\Delta L}$) is equal to or less than zero. A number of amino acids can be metabolized by cells and converted into lactic acid under tissue culture conditions [61,63,64]. In this case, the amount of lactate produced will be higher than the amount of glucose reacted, resulting in positive values of $\Sigma_{\Delta G,\Delta L}$. Our analysis shows that in control cell cultures grown in the absence of PA gels, $\Sigma_{\Delta G,\Delta L}$ is less than zero at all time points, as expected (Fig. 8A). In contrast, in cultures of cells with PA nanofibers $\Sigma_{\Delta G,\Delta L}$ was found to be positive at all time points (Fig. 8B). These observations suggest that cells entrapped in the gels are able to utilize the PA molecules in their metabolic pathways.

Our results show that MC3T3-E1 cells entrapped in PA matrices can survive for prolonged periods of time, and that entrapment does not arrest cell proliferation and motility. This observation together with results of our previous studies [9] demonstrate the suitability of PA gels for tissue engineering and cell entrapment. Our data also suggest that not all peptide sequences in PAs are equally appropriate for cell entrapment. It is not clear, at this point, why molecule **5** is toxic to MC3T3-E1 cells and continued studies of this observation are planned. While toxic PA molecules may not be useful for tissue engineering applications, they may however be useful in other applications such as cancer therapy. Finally, our results on glucose/lactate metabolism by MC3T3-E1 cells embedded in gels support TEM observations that nanofibers are endocytosed by the cells and indicate that nanofibers could be used as a source of nutrients.

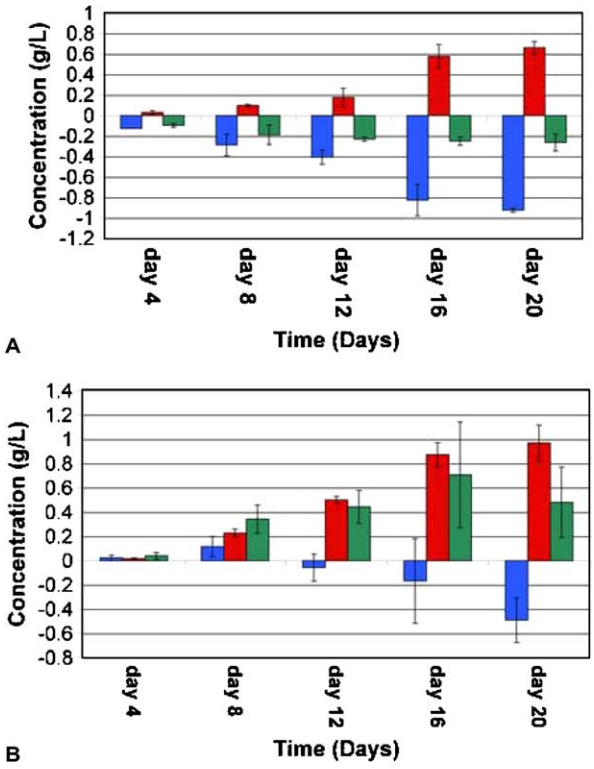

Fig. 8. Histograms showing changes in lactate ΔL (red) and glucose ΔG (blue) concentrations in control cultures (A) and cultures containing PA gels (B). Green bars correspond to the sum of ΔG and ΔL ($\Sigma_{\Delta G,\Delta L}$). Note that $\Sigma_{\Delta G,\Delta L}$ is negative in controls and positive in the experiments with PA gels, implying that there is a source other than glucose for lactate production. (For interpretation of the references in color in this figure legend, the reader is referred to the web version of this article.)

4. Conclusions

Peptide amphiphile molecules can assemble into robust nanofibrillar networks at physiological pH with the addition of polyvalent metal ions, and in some cases in the presence of monovalent ions. These nanostructured networks can therefore form in the presence of tissue fluids or cell culture media that contain these ions. Cells entrapped in the networks can survive and proliferate, and also internalize the nanofibers likely for use in metabolic pathways. The nanofiber networks could be useful in biotechnology applications, including cell transplantation and tissue engineering.

Acknowledgements

This work was funded by the US Department of Energy (DOE) (grant no. DE-FG02-00ER45810) and the National Science Foundation (NSF) (grant no.

DMR-0108342). We thank the Electron Probe Instrumentation Center (Hitachi 8100 TEM microscope), Biological Imaging Facility (JEOL 100 TEM microscope), Keck Biophysics Facility (Molecular Devices Gemini EM fluorescence plate reader, Cary 500 UV–Vis spectrometer) and the Analytical Services Laboratory (Biorad FTIR spectrometer) at Northwestern University.

References

[1] Dujardin E, Mann S. Bio-inspired materials chemistry. Adv Mater 2002;14:775–88.
[2] Green D, Walsh D, Mann S, Oreffo ROC. The potential of biomimesis in bone tissue engineering: Lessons from the design and synthesis of invertebrate skeletons. Bone 2002;30:810–5.
[3] Fields GB, Lauer JL, Dori Y, Forns P, Yu YC, Tirrell M. Protein-like molecular architecture: Biomaterial applications for inducing cellular receptor binding and signal transduction. Biopolymers 1998;47:143–51.
[4] Liu JC, Heilshorn SC, Tirrell DA. Comparative cell response to artificial extracellular matrix proteins containing the RGD and CS5 cell-binding domains. Biomacromolecules 2004;5:497–504.
[5] Tirrell M, Kokkoli E, Biesalski M. The role of surface science in bioengineered materials. Surf Sci 2002;500:61–83.
[6] Hartgerink JD, Beniash E, Stupp SI. Self-assembly and mineralization of peptide-amphiphile nanofibers. Science 2001;294:1684–8.
[7] Hartgerink JD, Beniash E, Stupp SI. Peptide-amphiphile nanofibers: A versatile scaffold for the preparation of self-assembling materials. Proc Natl Acad Sci USA 2002;99:5133–8.
[8] Niece KL, Hartgerink JD, Donners JJM, Stupp SI. Self-assembly combining two bioactive peptide-amphiphile molecules into nanofibers by electrostatic attraction. J Am Chem Soc 2003;125:7146–7.
[9] Silva GA, Czeisler C, Niece KL, Beniash E, Harrington DA, Kessler JA, Stupp SI. Selective differentiation of neural progenitor cells by high-epitope density nanofibers. Science 2004;303:1352–5.
[10] Timpl R, Brown JC. Supramolecular assembly of basement membranes. BioEssays 1996;18:123–32.
[11] Kadler KE, Holmes DF, Trotter JA, Chapman JA. Collagen fibril formation. Biochem J 1996;316:1–11.
[12] Fincham AG, Moradianoldak J, Simmer JP, Sarte P, Lau EC, Diekwisch T, Slavkin HC. Self-assembly of a recombinant amelogenin protein generates supramolecular structures. J Struct Biol 1994;112:103–9.
[13] Hwang JJ, Iyer SN, Li LS, Claussen R, Harrington DA, Stupp SI. Self-assembling biomaterials: Liquid crystal phases of cholesteryl oligo (L-lactic acid) and their interactions with cells. Proc Natl Acad Sci USA 2002;99:9662–7.
[14] Curtis A, Wilkinson C. Nantotechniques and approaches in biotechnology. Trend Biotechnol 2001;19:97–101.
[15] Lindsey JS. Self-assembly in synthetic routes to molecular devices—biological principles and chemical perspectives—a review. New J Chem 1991;15:153–80.
[16] Zhang SG. Fabrication of novel biomaterials through molecular self-assembly. Nat Biotechnol 2003;21:1171–8.
[17] Petka WA, Harden JL, McGrath KP, Wirtz D, Tirrell DA. Reversible hydrogels from self-assembling artificial proteins. Science 1998;281:389–92.
[18] Kaliyappan T, Kannan P. Co-ordination polymers. Prog Polym Sci 2000;25(3):343–70.
[19] Kurth DG, Caruso F, Schuler C. Giant self-contained metallo-supramolecular entities. Chem Commun 1999;16:1579–80.
[20] Buller R, Cohen H, Jensen TR, Kjaer K, Lahav M, Leiserowitz L. Self-assembly of bolaamphiphiles forming alternating layer arrangements with lead and copper divalent ions. J Phys Chem B 2001;105:11447–55.
[21] Allen R, Eisenberg S, Gray M. Quantitative measurement of the biological response of cartilage to mechanical deformation. In: Morgan J, Yarmush M, editors. Tissue engineering methods and protocols. Totowa, NJ: Humana; 1999.
[22] Kim Y-J, Sah R, Doong J-Y, Grodzinsky A. Fluorometric assay of DNA in cartilage explants using Hoechst 33258. Anal Biochem 1988;174:168–76.
[23] Kisiday J, Jin M, Kurz B, Hung H, Semino C, Zhang S, Grodzinsky AJ. Self-assembling peptide hydrogel fosters chondrocyte extracellular matrix production and cell division: Implications for cartilage tissue repair. Proc Natl Acad Sci USA 2002;99:9996–10001.
[24] Hauselmann HJ, Fernandes RJ, Mok SS, Schmid TM, Block JA, Aydelotte MB, Kuettner KE, Thonar E. Phenotypic stability of bovine articular chondrocytes after long-term culture in alginate beads. J Cell Sci 1994;107:17–27.
[25] Chen TH, Embree HD, Brown EM, Taylor MM, Payne GF. Enzyme-catalyzed gel formation of gelatin and chitosan: Potential for in situ applications. Biomaterials 2003;24:2831–41.
[26] Kong HJ, Wong E, Mooney DJ. Independent control of rigidity and toughness of polymeric hydrogels. Macromolecules 2003;36:4582–8.
[27] Caplan MR, Moore PN, Zhang SG, Kamm RD, Lauffenburger DA. Self-assembly of a beta-sheet protein governed by relief of electrostatic repulsion relative to van der Waals attraction. Biomacromolecules 2000;1:627–31.
[28] Caplan MR, Schwartzfarb EM, Zhang SG, Kamm RD, Lauffenburger DA. Control of self-assembling oligopeptide matrix formation through systematic variation of amino acid sequence. Biomaterials 2002;23:219–27.
[29] Zhang SG, Holmes T, Lockshin C, Rich A. Spontaneous assembly of a self-complementary oligopeptide to form a stable macroscopic membrane. Proc Natl Acad Sci USA 1993;90:3334–8.
[30] Leo WJ, McLoughlin AJ, Malone DM. Effects of sterilization treatments on some properties of alginate solutions and gels. Biotechnol Prog 1990;6:51–3.
[31] Draget KI, SkjakBraek G, Smidsrod O. Alginate based new materials. Int J Biol Macromol 1997;21:47–55.
[32] Bell JE, Hall C. UV and visible absorbance spectroscopy. In: Bell JE, editor. Spectroscopy in biochemistry. Boca Raton, FL: CRC Press; 1981. p. 3–62.
[33] Gray HB. Electronic absorption spectroscopy. In: Darnall DW, Wilkins RG, editors. Methods for determining metal ion environments in proteins: structure and function of metalloproteins. New York, NY: North-Holland; 1980. p. 1–23.
[34] Krimm S, Bandekar J. Vibrational spectroscopy and conformation of peptides, polypeptides, and proteins. Adv Protein Chem 1986;38:181–364.
[35] Kubelka J, Keiderling TA. Differentiation of beta-sheet-forming structures: Ab initio-based simulations of IR absorption and vibrational CD for model peptide and protein beta-sheets. J Am Chem Soc 2001;123:12048–58.
[36] Aggeli A, Bell M, Boden N, Keen JN, Knowles PF, McLeish TCB, Pitkeathly M, Radford SE. Responsive gels formed by the spontaneous self-assembly of peptides into polymeric beta-sheet tapes. Nature 1997;386:259–62.
[37] Pauling L, Corey RB, Branson HR. The structure of proteins-2 hydrogen-bonded helical configurations of the polypeptide chain. Proc Natl Acad Sci USA 1951;37:205–11.
[38] Gelbart WM, BenShaul A. The "new" science of complex fluids. J Phys Chem 1996;100:13169–89.

[39] Nagarajan R, Ruckenstein E. Theory of surfactant self-assembly—a predictive molecular thermodynamic approach. Langmuir 1991;7:2934–69.
[40] Israelachvili JN, Mitchell DJ, Ninham BW. Theory of self-assembly of hydrocarbon amphiphiles into micelles and bilayers. J Chem Soc-Faraday Trans II 1976;72:1525–68.
[41] Israelachvili JN, Mitchell DJ, Ninham BW. Theory of self-assembly of lipid bilayers and vesicles. Biochim Biophys Acta 1977;470:185–201.
[42] Tsonchev S, Troisi A, Schatz GC, Ratner MA. All-atom numerical studies of self-assembly of Zwitterionic peptide amphiphiles. J Phys Chem B 2004;108:15278–84.
[43] Tsonchev S, Schatz GC, Ratner MA. Electrostatically-directed self-assembly of cylindrical peptide amphiphile nanostructures. J Phys Chem B 2004;108:8817–22.
[44] Tsonchev S, Troisi A, Schatz GC, Ratner MA. On the structure and stability of self-assembled zwitterionic peptide amphiphiles: A theoretical study. Nano Lett 2004;4:427–31.
[45] Pierschbacher MD, Ruoslahti E. Cell attachment activity of fibronectin can be duplicated by small synthetic fragments of the molecule. Nature 1984;309:30–3.
[46] Hautanen A, Gailit J, Mann DM, Ruoslahti E. Effects of modifications of the RGD sequence and its context on recognition by the fibronectin. Receptor J Biol Chem 1989;264:1437–42.
[47] Freed LE, Vunjaknovakovic G, Marquis JC, Langer R. Kinetics of chondrocyte growth in cell-polymer implants. Biotechnol Bioeng 1994;43:597–604.
[48] Griffith LG, Naughton G. Tissue engineering-Current challenges and expanding opportunities. Science 2002;295:1009–14.
[49] Gambhir A, Europa AF, Hu WS. Alteration of cellular metabolism by consecutive fed-batch cultures of mammalian cells. J Biosci Bioeng 1999;87:805–10.
[50] Landis WJ, Hodgens KJ, Block D, Toma CD, Gerstenfeld LC. Spaceflight effects on cultured embryonic chick bone cells. J Bone Mineral Res 2000;15:1099–112.
[51] Rifas L, Gupta A, Hruska KA, Avioli LC. Altered osteoblast gluconeogenesis in X-linked hypophosphatemic mice is associated with a depressed intracellular Ph. Calcif Tissue Int 1995;57:60–3.
[52] Freshney RI. Culture of animal cells: a manual of basic technique. New York, NY: Alan R Liss; 1987.
[53] Lehninger AI. Principles of biochemistry. New York, NY: Worth Publishers; 1982.
[54] Zielke HR, Ozand PT, Tildon JT, Sevdalian DT, Cornblath M. Growth of human diploid fibroblasts in absence of glucose utilization. Proc Natl Acad Sci USA 1976;73:4110–4.
[55] Zielke HR, Ozand PT, Tildon JT, Sevdalian DT, Cornblath M. Reciprocal regulation of glucose and glutamine utilization by cultured human diploid fibroblasts. J Cell Phys 1978;95:41–8.
[56] Hu WS, Zhou WC, Europa LF. Controlling mammalian cell metabolism in bioreactors. J Microbiol Biotechnol 1998;8: 8–13.
[57] Guardia MJ, Gambhir A, Europa AF, Ramkrishna D, Hu WS. Cybernetic modeling and regulation of metabolic pathways in multiple steady states of hybridoma cells. Biotechnol Prog 2000;16:847–53.
[58] Gerecht-Nir S, Cohen S, Itskovitz-Eldor J. Bioreactor cultivation enhances the efficiency of human embryoid body (hEB) formation and differentiation. Biotechnol Bioeng 2004;86:493–502.
[59] Chiarini A, Petrini P, Bozzini S, Dal Pra I, Armato U. Silk fibroin/poly (carbonate)-urethane as a substrate for cell growth: In vitro interactions with human cells. Biomaterials 2003;24:789–99.
[60] Carrier RL, Papadaki M, Rupnick M, Schoen FJ, Bursac N, Langer R, Freed LE, Vunjak-Novakovic G. Cardiac tissue engineering: Cell seeding, cultivation parameters, and tissue construct characterization. Biotechnol Bioeng 1999;64:580–9.
[61] Gambhir A, Korke R, Lee JC, Fu PC, Europa A, Hu WS. Analysis of cellular metabolism of hybridoma cells at distinct physiological states. J Biosci Bioeng 2003;95:317–27.
[62] Dal Pra I, Petrini P, Charini A, Bozzini S, Fare S, Armato U. Silk fibroin-coated three-dimensional polyurethane scaffolds for tissue engineering: Interactions with normal human fibroblasts. Tissue Eng 2003;9:1113–21.
[63] Heidemann R et al. The use of peptones as medium additives for the production of a recombinant therapeutic protein in high density perfusion cultures of mammalian cells. Cytotechnology 2000;32:157–67.
[64] Nyberg GB, Balcarcel RR, Follstad BD, Stephanopoulos G, Wang DIC. Metabolism of peptide amino acids by Chinese hamster ovary cells grown in a complex medium. Biotechnol Bioeng 1999;62:324–35.